INTERNATIONAL JOURNAL FOR NUMERICAL METHODS IN ENGINEERING
Int. J. Numer. Meth. Engng 2007; **71**:1342–1364
Published online 29 January 2007 in Wiley InterScience (www.interscience.wiley.com). DOI: 10.1002/nme.1996

A discontinuous Galerkin method for a hyperbolic model for convection–diffusion problems in CFD

H. Gómez, I. Colominas*,†, F. Navarrina and M. Casteleiro

Group of Numerical Methods in Engineering, GMNI, Department of Applied Mathematics, Civil Engineering School, Universidad de A Coruña, Campus de Elviña, 15071 A Coruña, Spain

SUMMARY

This paper proposes a hyperbolic model for convection–diffusion transport problems in computational fluid dynamics (CFD). The hyperbolic model is based on the so-called Cattaneo's law. This is a time-dependent generalization of Fick's and Fourier's laws that was originally proposed to solve pure-diffusive heat transfer problems. We show that the proposed model avoids the infinite speed paradox that is inherent in the standard parabolic model.

A high-order upwind discontinuous Galerkin (DG) method is developed and applied to classic convection-dominated test problems. The quality of the numerical results is remarkable, since the discontinuities are very well captured without the appearance of spurious oscillations. These results are compared with those obtained by using the standard parabolic model and the local DG (LDG) method and with those given by the parabolic model and the Bassi–Rebay scheme.

Finally, the applicability of the proposed methodology is demonstrated by solving a practical case in engineering. We simulate the evolution of pollutant being spilled in the harbour of A Coruña (northwest of Spain, EU). Copyright © 2007 John Wiley & Sons, Ltd.

Received 11 May 2006; Revised 19 December 2006; Accepted 20 December 2006

KEY WORDS: convection–diffusion; Cattaneo's equation; finite speed; hyperbolic diffusion; discontinuous Galerkin

*Correspondence to: I. Colominas, E. T. S. de Ingenieros de Caminos, Canales y Puertos, Universidad de A Coruña, Campus de Elviña, 15071 A Coruña, Spain.
†E-mail: icolominas@udc.es

Contract/grant sponsor: Subdirección Xeral de I+D de la Xunta de Galicia; contract/grant numbers: PGIDT03PXIC18001PN, PGIDT05PXIC18002PN
Contract/grant sponsor: Ministerio de Educación y Ciencia; contract/grant numbers: DPI2002-00297, DPI2004-05156
Contract/grant sponsor: Universidade da Coruña
Contract/grant sponsor: Fundación de la Ingeniería Civil de Galicia

1. INTRODUCTION

The discontinuous Galarkin (DG) method is usually attributed to Reed and Hill [1]. Since its introduction in the framework of transport of neutrons in 1973, DG methods have evolved in a manner that made them suitable for computational fluid dynamics (CFD) [2]. The present popularity of the method is mainly due to Cockburn and Shu (with several collaborators) who introduced the Runge–Kutta DG method [3–6].

Whereas the continuous finite element methods were initially developed for elliptic equations, the DG method was primarily applied to hyperbolic problems. However, there has been extensive research lately into parabolic and elliptic DG methods [7–12]. Probably, the first successful study is due to Bassi and Rebay [7] who treated the viscous term in the Navier–Stokes equations within the DG framework. This method was followed by a paper by Cockburn and Shu [8] introducing the local DG (LDG) method. To use any of these two methods it is necessary to split the second-order Navier–Stokes (or convection–diffusion) equations in a system of first-order equations. Then, a DG-type discretization is used for both resulting equations. This procedure works quite well, but it introduces a number of extra degrees of freedom.

In this paper we propose a hyperbolic model for convection–diffusion problems that avoid the infinite speed paradox that is inherent in the parabolic formulation. The proposed model is based on the so-called Cattaneo's law [13, 14]. This is a time-dependent generalization of Fick's and Fourier's laws that was originally proposed to solve pure-diffusive heat transfer problems.

Furthermore, a high-order DG method is developed to solve the proposed model. We apply this numerical model to the resolution of classic convection-dominated test problems. The quality of the numerical results is remarkable, since the discontinuities are very well captured, without the appearance of spurious oscillations.

The outline of this paper is as follows: In Section 2 we review the classic formulation of the convective–diffusive equation. In Section 3 we study the formulation of the transport problem by using a Cattaneo-type law. A DG method for the resolution of the proposed convection–diffusion model is presented in Section 4. In Section 5 we solve some classic convection-dominated test problems by using the hyperbolic model and the proposed DG method. These results are compared with those obtained by using the standard parabolic model and the LDG method and with those given by the parabolic model and the Bassi–Rebay scheme. Finally, a practical case in engineering concerning the evolution of a pollutant spilled in the port of A Coruña (northwest of Spain, EU) is presented in Section 6. The main conclusions of this study are gathered in Section 7.

2. STANDARD FORMULATION OF THE CONVECTION–DIFFUSION TRANSPORT PROBLEM

2.1. Problem statement

In this section we review the classic formulation for the convection–diffusion transport problem. We assume the fluid medium to be incompressible and we do not consider source terms. The governing equations under these hypotheses are as follows:

$$\frac{\partial u}{\partial t} + \mathbf{a} \cdot \nabla_{\mathbf{x}} (u) + \nabla_{\mathbf{x}} \cdot (\mathbf{q}) = 0 \tag{1a}$$

$$\mathbf{q} = -\mathbf{K} \nabla_{\mathbf{x}} (u) \tag{1b}$$

DOI: 10.1002/nme

where u is the pollutant concentration, $\mathbf{a}$ is the velocity field which satisfies the hydrodynamic equations of the incompressible fluid, $\mathbf{q}$ is the pollutant flux per unit fluid density and $\mathbf{K}$ is the diffusivity tensor which is assumed to be positive definite. In the above system, (1a) and (1b) are the so-called equilibrium equation and constitutive equation, respectively. The equilibrium equation deals with the mass conservation. On the other side, the constitutive equation models how the diffusive transport is created in response to the variations in the pollutant distribution. This constitutive equation is known as Fick's law and its use is very frequent in engineering.

Clearly, system (1) can be decoupled since we can introduce (1b) into (1a) and solve the scalar equation

$$\frac{\partial u}{\partial t} + \mathbf{a} \cdot \nabla_{\mathbf{x}}(u) - \nabla_{\mathbf{x}} \cdot (\mathbf{K} \nabla_{\mathbf{x}}(u)) = 0 \tag{2}$$

It is well known that Equation (2) is parabolic. Therefore, boundary conditions must be imposed everywhere on the boundary of the domain [15].

Let us consider now the transport by convection and diffusion in a domain $\Omega \subset \mathbb{R}^2$ with piecewise smooth boundary Γ. The unit outward normal vector to Γ is denoted by $\mathbf{n}$. The boundary is assumed to consist of a portion Γ_{D} on which the value of u is prescribed (Dirichlet or essential conditions) and a complementary portion Γ_{N} on which the pollutant flux is prescribed (Neumann or natural conditions). In addition, we know the initial distribution of the transported quantity u. At this point we can state the convection–diffusion initial-boundary value problem as follows: given a divergence free velocity field $\mathbf{a}$, given the diffusion tensor $\mathbf{K}$ and given adequate initial and boundary conditions, find $u: \Omega \times [0, T] \mapsto \mathbb{R}$ such that

$$\frac{\partial u}{\partial t} + \mathbf{a} \cdot \nabla_{\mathbf{x}}(u) - \nabla_{\mathbf{x}} \cdot (\mathbf{K} \nabla_{\mathbf{x}}(u)) = 0 \quad \text{in } \Omega \times (0, T] \tag{3a}$$

$$u(\mathbf{x}, 0) = u_0(\mathbf{x}) \quad \text{on } \Omega \tag{3b}$$

$$u = u_{\mathrm{D}} \quad \text{on } \Gamma_{\mathrm{D}} \times (0, T] \tag{3c}$$

$$\mathbf{K} \nabla_{\mathbf{x}}(u) \cdot \mathbf{n} = h \quad \text{on } \Gamma_{\mathrm{N}} \times (0, T] \tag{3d}$$

2.2. A pure-diffusive example to analyse the infinite speed paradox

In what follows we will show that the above formulation leads to mass propagation at an infinite speed. Let us consider an (incompressible) homogeneous, isotropic (hence, if $\mathbf{I}$ is the identity tensor, $\mathbf{K} = k\mathbf{I}$ for a certain $k > 0$) and 1D medium. We consider a pure-diffusive situation and no source terms. We suppose the domain to be infinitely long. Therefore, no boundary conditions must be imposed. Finally, we assume that the pollutant is added to the medium as a rapid punctual pulse. In this case we should solve the following problem: find $u: \mathbb{R} \times [0, \infty) \mapsto \mathbb{R}$ such that

$$\frac{\partial u}{\partial t} - k \frac{\partial^2 u}{\partial x^2} = 0 \quad \forall x \in \mathbb{R}, \quad t > 0 \tag{4a}$$

$$u(x, 0) = \delta(x) \quad \forall x \in \mathbb{R} \tag{4b}$$

$$\lim_{x \to \pm\infty} u(x, t) = 0, \quad t > 0 \tag{4c}$$

DOI: 10.1002/nme

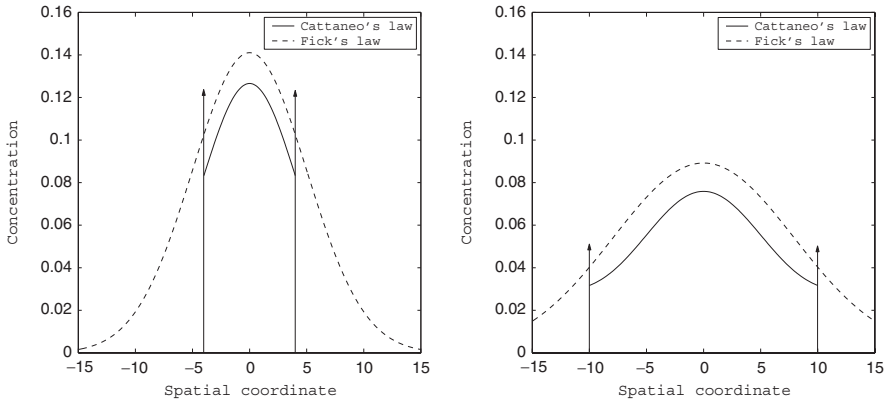

Figure 1. Comparison at $t=4$ (left) and at $t=10$ (right) between the solution of (4) (dashed line) and the solution of (8) (solid line). The vertical arrows represent Dirac's distributions. Parameters k and τ have a value of one.

where δ is the Dirac distribution. The exact solution of (4) is

$$u(x,t)=\frac{1}{\sqrt{4\pi kt}}\mathrm{e}^{-x^2/4kt} \quad \forall x\in\mathbb{R}, \quad t>0 \tag{5}$$

Therefore, for any given $t>0$, the pollutant distribution is given by the Gauss distribution function. The previous assertion implies that polluted fluid exists in the whole domain $\forall t>0$. However, at the initial time $u(x,0)=0\ \forall x\neq 0$, i.e. there is pollutant only in the origin of co-ordinates. Hence, a pollutant particle placed in x at time t must have reached the average velocity x/t in its trajectory. Since x/t is not bounded because the above assertion holds $\forall t>0$ and $\forall x\in\mathbb{R}$ we say that the speed of propagation is infinite. Figure 1 shows (in dashed line) the solution of (4) for $k=1$ at $t=4$ and 10.

3. A HYPERBOLIC FORMULATION FOR CONVECTION–DIFFUSION TRANSPORT PROBLEMS

3.1. Problem statement

We will derive this formulation by replacing Equation (1b) (Fick's law) by a Cattaneo-type law. Cattaneo's equation involves a tensorial function $\boldsymbol{\tau}$ called *relaxation tensor*. The components of the relaxation tensor are specific diffusion process times. Cattaneo's law was originally proposed for pure-diffusive problems and it takes the form:

$$\mathbf{q}+\boldsymbol{\tau}\frac{\partial\mathbf{q}}{\partial t}=-\mathbf{K}\nabla_{\mathbf{x}}(u) \tag{6}$$

Cattaneo's equation cannot be used in its original form for convection–diffusion problems because the resulting model would not fulfill the Galilean invariance principle [16, 17]. It is also expected that the total velocity of a pollutant that is being propagated at a finite speed in a fluid is the sum of the fluid velocity plus the velocity of the pollutant. This is not verified if we use

DOI: 10.1002/nme

the original form of Cattaneo's law. To address these problems we proposed to modify Cattaneo's law by imposing the Galilean invariance principle to the model [16, 18, 19]. Thus, the description of the diffusion process is granted to be the same in every inertial frame. By doing so, the basic equations for the transport problem described by using a Cattaneo-type law are found to be

$$\frac{\partial u}{\partial t} + \mathbf{a} \cdot \nabla_{\mathbf{x}}(u) + \nabla_{\mathbf{x}} \cdot (\mathbf{q}) = 0 \tag{7a}$$

$$\mathbf{q} + \boldsymbol{\tau}\left(\frac{\partial \mathbf{q}}{\partial t} + \nabla_{\mathbf{x}}(\mathbf{q})\mathbf{a}\right) = -\mathbf{K}\nabla_{\mathbf{x}}(u) \tag{7b}$$

where (7b) is Cattaneo's law with convective term. It should be noted that we are proposing a generalized constitutive equation. In fact, we recover the classic parabolic formulation when $\boldsymbol{\tau} = 0$.

3.2. A pure-diffusive example with a finite velocity of propagation

In order to compare the solution of the classic formulation with the solution of the generalized formulation we now solve the hyperbolic counterpart of (4). In this simple case, system (7) can be written as a single second-order partial differential equation (for further details, see [16]). Now, we need two initial conditions because this problem involves second-order derivatives with respect to the time. Then, we consider an (incompressible) homogeneous, isotropic (hence, $\mathbf{K} = k\mathbf{I}$, $\boldsymbol{\tau} = \tau\mathbf{I}$ for certain $k, \tau \in \mathbb{R}^+$), 1D and non-convective medium. With the above hypotheses we can state this problem as: find $u: \mathbb{R} \times [0, \infty) \mapsto \mathbb{R}$ such that

$$\tau\frac{\partial^2 u}{\partial t^2} + \frac{\partial u}{\partial t} - k\frac{\partial^2 u}{\partial x^2} = 0 \quad \forall x \in \mathbb{R}, \quad t > 0 \tag{8a}$$

$$u(x, 0) = \delta(x) \quad \forall x \in \mathbb{R} \tag{8b}$$

$$\frac{\partial u}{\partial t}(x, 0) = 0 \quad \forall x \in \mathbb{R} \tag{8c}$$

$$\lim_{x \to \pm\infty} u(x, t) = 0, \quad t > 0 \tag{8d}$$

We may solve (8) by using subsequent Laplace and Fourier transforms (see Reference [16] for a detailed resolution). By these means, we obtain

$$u(x, t) = \begin{cases} \dfrac{1}{2}\mathrm{e}^{-c^2/2kt}\left[\delta(|x| - ct) + \dfrac{c}{2k} I_0\left(\dfrac{c}{2k}\sqrt{c^2t^2 - x^2}\right) + \dfrac{c^2}{2k} t \dfrac{I_1\left(\frac{c}{2k}\sqrt{c^2t^2 - x^2}\right)}{\sqrt{c^2t^2 - x^2}}\right], & |x| \leqslant ct \\ 0, & |x| > ct \end{cases} \tag{9}$$

where I_0 and I_1 are the modified Bessel functions of the first kind of order 0 and 1. Furthermore, c is what we call *mass wave celerity*, being defined as

$$c = \sqrt{k/\tau} \tag{10}$$

In Figure 1 we compare the solutions to (4) and (8) at $t = 4$ and 10, respectively. We remark that Cattaneo's equation predicts the existence of a wave front which advances with a celerity c.

DOI: 10.1002/nme

3.3. Study of the proposed model as a system of conservation laws

System (7) cannot be written as a single second-order partial differential equation in multidimensional problems with a non-constant velocity field [16]. In this case we must solve a coupled system of first-order partial differential equations. If we introduce the hypothesis that $\boldsymbol{\tau}$ is a regular matrix (this appears to be reasonable; in fact, it seems natural to demand $\boldsymbol{\tau}$ to be positive-definite since it is representing a characteristic time of the diffusion process) and we use again that the fluid medium is incompressible, system (7) can be written as a system of conservation laws as follows:

$$\frac{\partial u}{\partial t} + \nabla_{\mathbf{x}} \cdot (u\mathbf{a} + \mathbf{q}) = 0 \tag{11a}$$

$$\frac{\partial \mathbf{q}}{\partial t} + \nabla_{\mathbf{x}} \cdot (\mathbf{q} \otimes \mathbf{a} + \boldsymbol{\tau}^{-1}\mathbf{K}u) = u\nabla_{\mathbf{x}} \cdot (\boldsymbol{\tau}^{-1}\mathbf{K}) - \boldsymbol{\tau}^{-1}\mathbf{q} \tag{11b}$$

For the sake of simplicity we will consider from here on the medium to be homogeneous, isotropic and 2D. Under these hypotheses, system (7) can be written as [18, 20]

$$\frac{\partial \mathbf{U}}{\partial t} + \nabla_{\mathbf{x}} \cdot (\mathbf{F}) = \mathbf{S} \tag{12}$$

where vectors $\mathbf{U}$, $\mathbf{S}$ and the conservation flux function $\mathbf{F}$ take the form

$$\mathbf{U} = \begin{pmatrix} u \\ \tau q_1 \\ \tau q_2 \end{pmatrix}, \quad \mathbf{F} = \begin{pmatrix} ua_1 + q_1 & ua_2 + q_2 \\ \tau q_1 a_1 + ku & \tau q_1 a_2 \\ \tau q_2 a_1 & \tau q_2 a_2 + ku \end{pmatrix}, \quad \mathbf{S} = \begin{pmatrix} 0 \\ -q_1 \\ -q_2 \end{pmatrix} \tag{13}$$

The notation $\mathbf{q} = (q_1, q_2)^{\mathrm{T}}$, $\mathbf{a} = (a_1, a_2)^{\mathrm{T}}$ has also been used.

In order to study the basic properties of Equation (12) it is necessary to rewrite it in a non-conservative form. In this way, if we define $\mathbf{F}_i$ as the ith column of matrix $\mathbf{F}$, the following relation holds:

$$\nabla_{\mathbf{x}} \cdot (\mathbf{F}) = \frac{\partial \mathbf{F}_1}{\partial x_1} + \frac{\partial \mathbf{F}_2}{\partial x_2} = \mathbf{A}_1 \frac{\partial \mathbf{U}}{\partial x_1} + \mathbf{A}_2 \frac{\partial \mathbf{U}}{\partial x_2} \tag{14}$$

$\mathbf{A}_1$ and $\mathbf{A}_2$ being the Jacobian matrices defined by

$$\mathbf{A}_1 = \nabla_{\mathbf{U}}(\mathbf{F}_1) = \begin{pmatrix} a_1 & 1/\tau & 0 \\ k & a_1 & 0 \\ 0 & 0 & a_1 \end{pmatrix}, \quad \mathbf{A}_2 = \nabla_{\mathbf{U}}(\mathbf{F}_2) = \begin{pmatrix} a_2 & 0 & 1/\tau \\ 0 & a_2 & 0 \\ k & 0 & a_2 \end{pmatrix} \tag{15}$$

Now, we define the vector of matrices (hypermatrix) $\mathbf{A}^{\mathrm{T}} = (\mathbf{A}_1, \mathbf{A}_2)$. This definition allows us to use the notation $\nabla_{\mathbf{x}} \cdot (\mathbf{F}) = (\mathbf{A} \cdot \nabla_{\mathbf{x}})\mathbf{U}$ and to rewrite (12) as

$$\frac{\partial \mathbf{U}}{\partial t} + (\mathbf{A} \cdot \nabla_{\mathbf{x}})\mathbf{U} = \mathbf{S} \tag{16}$$

DOI: 10.1002/nme

which is a linear system of equations since $\mathbf{A}$ does not depend on $\mathbf{U}$. Now, we define $\boldsymbol{\kappa} = (\kappa_1, \kappa_2)^{\mathrm{T}}$ as an arbitrary vector with the constriction $\|\boldsymbol{\kappa}\| = 1$, where $\|\cdot\|$ denotes the Euclidean norm of a given vector. It can be shown that (16) is totally hyperbolic if the equation

$$\det(\omega \mathbf{I} - \mathbf{A} \cdot \boldsymbol{\kappa}) = 0 \tag{17}$$

yields three different real solutions ω for arbitrarily prescribed values of $\boldsymbol{\kappa}$ [15]. It is easy to prove that Equation (17) has the three different solutions

$$\omega_1 = \mathbf{a} \cdot \boldsymbol{\kappa} \tag{18a}$$

$$\omega_2 = \mathbf{a} \cdot \boldsymbol{\kappa} - c \tag{18b}$$

$$\omega_3 = \mathbf{a} \cdot \boldsymbol{\kappa} + c \tag{18c}$$

In addition, the values written in (18) are the eigenvalues of $\mathbf{A} \cdot \boldsymbol{\kappa}$ which is usually referred to as the *projection matrix*. Now, by making some basic algebraic work we can compute the eigenvectors of $\mathbf{A} \cdot \boldsymbol{\kappa}$. Then, we can define the square matrix $\mathbf{C}$ as the matrix whose columns are the eigenvectors of the projection matrix, that is,

$$\mathbf{C} = \begin{pmatrix} 0 & c & c \\ \kappa_2 & -k\kappa_1 & k\kappa_1 \\ -\kappa_1 & -k\kappa_2 & k\kappa_2 \end{pmatrix} \tag{19}$$

Let $\mathbf{D}$ be the diagonal matrix such that the elements placed in the main diagonal are the eigenvalues $\omega_1, \omega_2, \omega_3$. Then, the following relation holds:

$$\mathbf{D} = \mathbf{C}^{-1}(\mathbf{A} \cdot \boldsymbol{\kappa})\mathbf{C} \tag{20}$$

It is important to note that matrices $\mathbf{A}_1$ and $\mathbf{A}_2$ are not diagonalizable in the same base. Therefore, system (16) cannot be diagonalized. Thus, it is not possible to define Riemann quasi-invariants in 2D and 3D problems but only in 1D problems [18]. At this point, it is useful to introduce the following dimensionless number:

$$H = \frac{\|\mathbf{a}\|}{c} \tag{21}$$

which plays a similar role in the Mach number in compressible flow problems [21] or to the Froude number in shallow water problems [22]. By using this dimensionless number we can differentiate three kinds of flow

- $H < 1 \Leftrightarrow$ subcritical flow;
- $H > 1 \Leftrightarrow$ supercritical flow;
- $H = 1 \Leftrightarrow$ critical flow.

It should be noted that upstream pollutant transport is not possible in supercritical flow conditions, since the velocity of the diffusive mode of propagation is smaller than the velocity of the convective mode.

DOI: 10.1002/nme

3.4. Boundary conditions

Imposing boundary conditions for system (16) is not trivial. Further, an inadequate choice could affect the existence and uniqueness of solution to this problem. A quite frequent easy type of boundary condition is the one that corresponds to a fixed solid wall. In this situation only the normal component of the pollutant flux $\mathbf{q}$ must be prescribed. Thus, the boundary condition in this case will be $\mathbf{q} \cdot \mathbf{n} = 0$. However, computational domains are usually limited by other kinds of boundaries, as well. These are the so-called inflow and outflow boundaries. In these types of boundaries the issue of properly defining boundary conditions is more complicated. It is well known that boundary conditions for scalar hyperbolic problems are only imposed on the inflow part of the boundary. For systems of hyperbolic equations only inflow components can be prescribed. As a consequence of that, a Riemann analysis in the direction of the outward normal is necessary. It has been shown that Cattaneo-type transport equations can be diagonalized in 1D, although they remain coupled by the source term. Thus, the 2D equations can be diagonalized in the direction of the outward normal to the boundary. In this way, three different velocities of propagation are found:

$$\omega_1 = \mathbf{a} \cdot \mathbf{n} \tag{22a}$$

$$\omega_2 = \mathbf{a} \cdot \mathbf{n} - c \tag{22b}$$

$$\omega_3 = \mathbf{a} \cdot \mathbf{n} + c \tag{22c}$$

In order to obtain a well-posed problem it is necessary to impose as many of components of $\mathbf{U}$ as the number of negative velocities (incoming information) given by (22). Therefore, in a supercritical inflow boundary all components of $\mathbf{U}$ must be prescribed while no components should be imposed in a supercritical outflow boundary. In contrast, in a subcritical outflow boundary only one component of $\mathbf{U}$ must be prescribed while two components of $\mathbf{U}$ should be imposed in a subcritical inflow boundary. On the other hand, an initial condition must be imposed to (16) independently of the boundary conditions. Consequently, the 2D Cattaneo-type transport problem can be stated as follows: Given $k, \tau > 0$, given a divergence-free velocity field $\mathbf{a}$ and given adequate initial and boundary conditions, find $\mathbf{U}: \Omega \times [0, T] \mapsto \mathbb{R}^2$ such that

$$\frac{\partial \mathbf{U}}{\partial t} + \nabla_{\mathbf{x}} \cdot (\mathbf{F}) = \mathbf{S} \quad \text{in } \Omega \times [0, T] \tag{23a}$$

$$\mathbf{U}(x, 0) = \mathbf{U}_0(x) \quad \text{on } \Omega \tag{23b}$$

$$\mathbf{U}^{\text{in}} = \mathbf{U}_{\text{D}}^{\text{in}} \quad \text{on } \Gamma_{\text{D}} \times [0, T] \tag{23c}$$

$$\mathbf{F}^{\text{in}} \mathbf{n} = \mathbf{F}_{\text{N}} \quad \text{on } \Gamma_{\text{N}} \times [0, T] \tag{23d}$$

$\mathbf{F}$, $\mathbf{S}$ being the vectors defined in (13), $\mathbf{U}^{\text{in}}$ the inflow components of $\mathbf{U}$ and $\mathbf{F}^{\text{in}}$ the inflow components of the conservation flux matrix.

4. DG FORMULATION OF THE PROPOSED MODEL

In this section a DG method for the hyperbolic convection–diffusion equation is presented. The formulation is identical for 2D and 3D problems. From here on, we will restrict to the 2D problem

DOI: 10.1002/nme

in order to simplify the exposition. The system to be solved is (23) with adequate initial and boundary conditions. Let Ω^h be a partition of the computational domain Ω into a mesh of $n$elem elements. Let $\Omega_{i\text{elem}}$ be a general element with boundary $\Gamma_{i\text{elem}}$. We also define the following set of polynomials:

$$\mathscr{V}^h = \{v^h \in \mathscr{L}^2(\Omega) : v^h|_{\Omega_{i\text{elem}}} \in \mathscr{P}^m(\Omega_{i\text{elem}}), \forall \Omega_{i\text{elem}} \in \Omega^h\} \tag{24}$$

where $\mathscr{P}^m(\Omega_{i\text{elem}})$ is the space of polynomials of degree at most m. Note that the discrete space does not enforce $\mathscr{C}^0$ continuity and that m, in general, can vary in all elements. Taking into account all of this, we can derive the variational formulation of the problem by multiplying the governing equation with a smooth test function w and by integrating over the local element $\Omega_{i\text{elem}}$:

$$\int\int_{\Omega_{i\text{elem}}} w\frac{\partial \mathbf{U}}{\partial t}\,\mathrm{d}\Omega + \int\int_{\Omega_{i\text{elem}}} w\nabla_{\mathbf{x}}\cdot(\mathbf{F})\,\mathrm{d}\Omega = \int\int_{\Omega_{i\text{elem}}} w\mathbf{S}\,\mathrm{d}\Omega \tag{25}$$

In order to obtain the discrete Galerkin formulation we approximate $\mathbf{U}$ by a polynomial expansion $\mathbf{U}^h \in \mathscr{V}^h$. Further, we restrict the class of test functions to those $w^h \in \mathscr{V}^h$. In addition, we integrate by parts the second term in (25). By these means, we find the expression

$$\int\int_{\Omega_{i\text{elem}}} w^h\frac{\partial \mathbf{U}^h}{\partial t}\,\mathrm{d}\Omega - \int\int_{\Omega_{i\text{elem}}} \mathbf{F}^h\nabla_{\mathbf{x}}(w^h)\,\mathrm{d}\Omega + \int_{\Gamma_{i\text{elem}}} w^h\mathbf{F}^h\cdot\mathbf{n}\,\mathrm{d}\Gamma = \int\int_{\Omega_{i\text{elem}}} w^h\mathbf{S}^h\,\mathrm{d}\Omega \tag{26}$$

Due to the discontinuous representation of the solution in the DG method, two values of the unknown $\mathbf{U}^h$ exist over the edges of the elements. For this reason, we substitute the discontinuous boundary flux term $\mathbf{F}^h\cdot\mathbf{n}$ for a continuous numerical flux denoted by $\widehat{\mathbf{F}}\cdot\mathbf{n}$. The numerical flux is constructed taking into account the two values of $\mathbf{U}^h$ that exist over the edges of the elements. These two values are combined in order to design the numerical flux according to the direction of propagation of the flow.

4.1. Numerical flux

Over each edge $L_{i\text{edge}}$ of the element $\Omega_{i\text{elem}}$ the boundary flux can be written as $\mathbf{F}^h\cdot\mathbf{n}_{i\text{edge}} = \mathbf{A}\cdot\mathbf{n}_{i\text{edge}}\mathbf{U}^h$ where $\mathbf{A}^{\mathrm{T}} = (\mathbf{A}_1, \mathbf{A}_2)$ is a hypermatrix and $\mathbf{n}_{i\text{edge}}$ is the unit outward normal to $L_{i\text{edge}}$. Thus, over each edge $L_{i\text{edge}}$ it is possible (due to the hyperbolicity of the system) to diagonalize the matrix $\mathbf{A}\cdot\mathbf{n}_{i\text{edge}}$ as follows:

$$\mathbf{A}\cdot\mathbf{n}_{i\text{edge}} = \mathbf{C}_{i\text{edge}}\mathbf{D}_{i\text{edge}}\mathbf{C}^{-1}_{i\text{edge}} \tag{27}$$

where matrices $\mathbf{C}$ and $\mathbf{D}$ have been defined in (19) and (20) for a given direction $\boldsymbol{\kappa}$. Now, we split the matrix $\mathbf{D}_{i\text{edge}}$ as

$$\mathbf{D}_{i\text{edge}} = \mathbf{D}^+_{i\text{edge}} + \mathbf{D}^-_{i\text{edge}} \tag{28}$$

DOI: 10.1002/nme

being

$$\mathbf{D}^{\pm}_{i\text{edge}} = \begin{pmatrix} \dfrac{\mathbf{a}\cdot\mathbf{n}_{i\text{edge}} \pm |\mathbf{a}\cdot\mathbf{n}_{i\text{edge}}|}{2} & 0 & 0 \\ 0 & \dfrac{\mathbf{a}\cdot\mathbf{n}_{i\text{edge}} - c \pm |\mathbf{a}\cdot\mathbf{n}_{i\text{edge}} - c|}{2} & 0 \\ 0 & 0 & \dfrac{\mathbf{a}\cdot\mathbf{n}_{i\text{edge}} + c \pm |\mathbf{a}\cdot\mathbf{n}_{i\text{edge}} + c|}{2} \end{pmatrix} \tag{29}$$

By these means, we can write

$$\mathbf{A}\cdot\mathbf{n}_{i\text{edge}} = \underbrace{\mathbf{C}_{i\text{edge}}\mathbf{D}^{+}_{i\text{edge}}\mathbf{C}^{-1}_{i\text{edge}}}_{\mathbf{A}^{+}_{i\text{edge}}} + \underbrace{\mathbf{C}_{i\text{edge}}\mathbf{D}^{-}_{i\text{edge}}\mathbf{C}^{-1}_{i\text{edge}}}_{\mathbf{A}^{-}_{i\text{edge}}} \tag{30}$$

and the upwind numerical flux over edge $L_{i\text{edge}}$ is found to be

$$\widehat{\mathbf{F}}\cdot\mathbf{n}_{i\text{edge}} = \mathbf{A}^{+}_{i\text{edge}}\mathbf{U}^{h}_{i\text{elem}} + \mathbf{A}^{-}_{i\text{edge}}\mathbf{U}^{h}_{i\text{elad}} \tag{31}$$

where Ω_{ielad} is the adjacent element to edge $L_{i\text{edge}}$ of element $\Omega_{i\text{elem}}$.

4.2. Interpolation

We use Lagrangian elements of $n\text{node}$ nodes. Therefore, for a given time t and for a given $\mathbf{x}\in\Omega_{i\text{elem}}$ we interpolate the solution as

$$\mathbf{U}^{h}(\mathbf{x},t)|_{\Omega_{i\text{elem}}} = \sum_{i\text{node}=1}^{n\text{node}} N^{i\text{node}}_{i\text{elem}}(\mathbf{x})\mathscr{U}^{i\text{node}}_{i\text{elem}}(t) \tag{32}$$

where $N^{i\text{node}}_{i\text{elem}}$ is the shape function associated with (local) node $i\text{node}$ of element $\Omega_{i\text{elem}}$. Using the interpolation given by (32) and the numerical flux defined in (31) we can rewrite (26) as follows:

$$\begin{aligned} &\sum_{i\text{node}=1}^{n\text{node}} \iint_{\Omega_{i\text{elem}}} N^{j\text{node}}_{i\text{elem}} N^{i\text{node}}_{i\text{elem}}\,\mathrm{d}\Omega \frac{\mathrm{d}}{\mathrm{d}t}(\mathscr{U}^{i\text{node}}_{i\text{elem}}) \\ &\quad= \sum_{i\text{node}=1}^{n\text{node}} \iint_{\Omega_{i\text{elem}}} \left(\frac{\partial N^{j\text{node}}_{i\text{elem}}}{\partial x_1} N^{i\text{node}}_{i\text{elem}}\mathbf{A}_1 + \frac{\partial N^{j\text{node}}_{i\text{elem}}}{\partial x_2} N^{i\text{node}}_{i\text{elem}}\mathbf{A}_2 + N^{j\text{node}}_{i\text{elem}} N^{i\text{node}}_{i\text{elem}}\mathbf{B} \right) \mathrm{d}\Omega \mathscr{U}^{i\text{node}}_{i\text{elem}} \\ &\qquad+ \sum_{i\text{node}=1}^{n\text{node}} \left[\sum_{i\text{edge}=1}^{n\text{edge}} \int_{L_{i\text{edge}}} -N^{j\text{node}}_{i\text{elem}} N^{i\text{node}}_{i\text{elem}} \mathbf{A}^{+}_{i\text{edge}}\,\mathrm{d}L \right] \mathscr{U}^{i\text{node}}_{i\text{elem}} \\ &\qquad+ \sum_{i\text{node}=1}^{n\text{node}} \left[\sum_{i\text{edge}=1}^{n\text{edge}} \int_{L_{i\text{edge}}} -N^{j\text{node}}_{i\text{elem}} N^{i\text{node}}_{i\text{lad}} \mathbf{A}^{-}_{i\text{edge}}\,\mathrm{d}L \mathscr{U}^{i\text{node}}_{i\text{elad}} \right] \quad \begin{matrix} \forall j\text{node}=1, n\text{node} \\ \forall i\text{elem}=1, n\text{elem} \end{matrix} \end{aligned} \tag{33}$$

DOI: 10.1002/nme

In the previous equation **B** is the Jacobian matrix associated with the source term, i.e.

$$\mathbf{B} = \nabla_{\mathbf{U}}(\mathbf{S}) = \begin{pmatrix} 0 & 0 & 0 \\ 0 & -1/\tau & 0 \\ 0 & 0 & -1/\tau \end{pmatrix} \tag{34}$$

From Equation (33) it is apparent that the domain of dependence of the method is minimal, since only first neighbours of the element $\Omega_{i\text{elem}}$ are involved. This fact allows a very efficient parallelization.

4.3. Numerical integration

In the 2D numerical examples that we present in this paper we have used biquadratic Lagrangian elements. Numerical integration is performed by using a 3×3 points Gauss–Legendre quadrature for the elemental integrals and a 3-point Gauss–Legendre integration for the boundary terms.

4.4. Time integration

By assembling together all the elemental contributions, the system of ordinary differential equations that governs the evolution of the discrete solution can be written as

$$\mathbf{M}\frac{\mathrm{d}\mathscr{U}}{\mathrm{d}t} = \mathbf{R}(\mathscr{U}) \tag{35}$$

where **M** denotes the mass matrix, $\mathscr{U}$ is the global vector of degrees of freedom and $\mathbf{R}(\mathscr{U})$ is the residual vector. Due to the block diagonal structure of matrix **M**, the time integration of this system can be accomplished in an efficient way by means of an explicit method for initial value problems. In this work we use the third-order TVD–Runge–Kutta method proposed by Shu and Osher [23]. Given the solution at the nth step ($\mathscr{U}^n$), the solution at the next time level ($\mathscr{U}^{n+1}$) is computed in three steps as follows:

$$\mathscr{U}^{(1)} = \mathscr{U}^n + \Delta t\mathbf{L}(\mathscr{U}^n) \tag{36a}$$

$$\mathscr{U}^{(2)} = \tfrac{3}{4}\mathscr{U}^n + \tfrac{1}{4}\mathscr{U}^{(1)} + \tfrac{1}{4}\Delta t\mathbf{L}(\mathscr{U}^{(1)}) \tag{36b}$$

$$\mathscr{U}^{n+1} = \tfrac{1}{3}\mathscr{U}^n + \tfrac{2}{3}\mathscr{U}^{(2)} + \tfrac{2}{3}\Delta t\mathbf{L}(\mathscr{U}^{(2)}) \tag{36c}$$

where $\mathbf{L}(\mathscr{U}) = \mathbf{M}^{-1}\mathbf{R}(\mathscr{U})$. To compute $\mathbf{L}(\mathscr{U})$ at each time step we do not need to calculate $\mathbf{M}^{-1}$. Instead of that, we compute the Cholesky factorization of the mass matrix at the first time step and we perform the necessary back and forward substitutions at each time iteration.

4.5. Boundary conditions

In the DG framework it is usual to impose boundary conditions in a weak form on both, inflow and outflow, boundaries. It is recognized by most authors that the weak imposition of Dirichlet-type conditions is superior to the strong imposition on outflow boundaries [24]. This is due to the appearance of spurious oscillations in boundary layers when Dirichlet boundary conditions are imposed strongly. However, the weak enforcement of inflow Dirichlet boundary conditions offers

DOI: 10.1002/nme

no advantages over the strong imposition [25]. As mentioned in Section 3.3, for the proposed hyperbolic convection–diffusion model, no boundary conditions should be imposed on supercritical outflow boundaries. This fact avoids the presence of boundary layers in the solution when convection dominates diffusion. For this reason, we enforce boundary conditions strongly for the hyperbolic model.

5. NUMERICAL EXAMPLES

In this section we present some numerical examples of the solution to the hyperbolic convection–diffusion equations by using the proposed DG scheme. We present both 1D and 2D examples.

5.1. One-dimensional problems

The model problem is the hyperbolic convection–diffusion equation in $\Omega = (0, 1)$. The flow is given by the parameters $k = 1$, $\tau = 1$ and $a = 0.5$ which make it to be subcritical. We consider the boundary conditions $u(0) = 0$, $u(1) = 1$ which can be imposed on subcritical flow conditions. We will use the presented DG method to compute the steady-state solution. Then, we will compare the numerical solution with the exact solution of the steady problem to obtain the error. The time step is taken small enough so that the error can be assumed to arise from the spatial discretization. Within each element we interpolate the solution by using polynomials of degree m. We present the results for $m = 1$ and 2. The optimal order of accuracy $(m + 1)$ is achieved in both concentration and pollutant flux as it can be seen in Tables I–IV.

Table I. $\|\cdot\|_\infty$ and $\|\cdot\|_2$ concentration errors and numerical order of accuracy.

Elements	$\|\mathbf{Error}\|_\infty$	Order$\|\cdot\|_\infty$	$\|\mathbf{Error}\|_2$	Order$\|\cdot\|_2$
5	$7.0149 \times 10{-}3$	—	2.9403×10^{-3}	—
10	1.9811×10^{-3}	1.83	7.9018×10^{-4}	1.90
20	5.2591×10^{-4}	1.92	2.1538×10^{-4}	1.88
40	1.3885×10^{-4}	1.93	5.6566×10^{-5}	1.93
80	3.5664×10^{-5}	1.96	1.4493×10^{-5}	1.97

Note: Linear elements. $k = 1$, $\tau = 1$, $a = 0.5$.

Table II. $\|\cdot\|_\infty$ and $\|\cdot\|_2$ pollutant flux errors and numerical order of accuracy.

Elements	$\|\mathbf{Error}\|_\infty$	Order $\|\cdot\|_\infty$	$\|\mathbf{Error}\|_2$	Order $\|\cdot\|_2$
5	1.5607×10^{-2}	—	9.1734×10^{-3}	—
10	3.8745×10^{-3}	2.01	2.3406×10^{-3}	1.97
20	1.0109×10^{-3}	1.94	5.9517×10^{-4}	1.98
40	2.6091×10^{-4}	1.96	1.5010×10^{-4}	1.99
80	6.6288×10^{-5}	1.98	3.7693×10^{-5}	2.00

Note: Linear elements. $k = 1$, $\tau = 1$, $a = 0.5$.

DOI: 10.1002/nme

Table III. $\|\cdot\|_\infty$ and $\|\cdot\|_2$ concentration errors and numerical order of accuracy.

Elements	$\|\mathbf{Error}\|_\infty$	Order $\|\cdot\|_\infty$	$\|\mathbf{Error}\|_2$	Order $\|\cdot\|_2$
5	1.2313×10^{-4}	—	6.5825×10^{-5}	—
10	1.5790×10^{-5}	2.96	8.6646×10^{-6}	2.93
20	2.0916×10^{-6}	2.92	1.1112×10^{-6}	2.96
40	2.6937×10^{-7}	2.96	1.4100×10^{-7}	2.98
80	3.4207×10^{-8}	2.98	1.7967×10^{-8}	2.98

Note: Quadratic elements. $k=1$, $\tau=1$, $a=0.5$.

Table IV. $\|\cdot\|_\infty$ and $\|\cdot\|_2$ pollutant flux errors and numerical order of accuracy.

Elements	$\|\mathbf{Error}\|_\infty$	Order $\|\cdot\|_\infty$	$\|\mathbf{Error}\|_2$	Order $\|\cdot\|_2$
5	1.4723×10^{-4}	—	5.0684×10^{-5}	—
10	1.8043×10^{-5}	3.03	5.7567×10^{-6}	3.14
20	2.3157×10^{-6}	2.97	6.3246×10^{-7}	3.19
40	2.9365×10^{-7}	2.98	7.2585×10^{-8}	3.13
80	3.7256×10^{-8}	2.98	8.5612×10^{-9}	3.08

Note: Quadratic elements. $k=1$, $\tau=1$, $a=0.5$.

In some cases the optimal order of accuracy is not exactly achieved, but it is due to the roundoff errors and to the tolerance in considering the solution to be steady.

5.2. Two-dimensional problems

In this section we solve some classic convection-dominated test problems by using the hyperbolic convection–diffusion model and the proposed DG method. These results are compared with those obtained by using the parabolic model and the LDG method or the Bassi–Rebay scheme for the spatial discretization. Roughly speaking, the LDG method and the Bassi–Rebay scheme consist in applying a DG-type discretization to both equations in system (1). In this way, the concentration u and its derivatives are treated as independent variables. A comprehensive study of the Bassi–Rebay method and the LDG scheme can be found in [7, 8], respectively.

5.2.1. Pure rotation in an irregular domain. We will solve the parabolic and the hyperbolic convection–diffusion models within the domain depicted in Figure 2. The velocity field is given by $\mathbf{a}=(-x_2, x_1)$ which defines a pure-rotation. The diffusivity is $k=10^{-6}$. For the hyperbolic model we take $\tau=1$ which makes the flow to be supercritical at each point of the domain. For the hyperbolic model we must impose no conditions on the outflow boundary while all the variables must be imposed on the inflow boundary. We impose $\mathbf{q}=0$ everywhere on the inflow boundary of the domain and a discontinuous concentration condition as it can be seen in Figure 2.

On the other hand, for the parabolic model we must impose a boundary condition everywhere on the boundary of the domain. On the inflow boundary we impose the concentration boundary condition that has been depicted in Figure 2. On the outflow boundary we impose the condition $\mathbf{q}\cdot\mathbf{n}=0$ in order to avoid the appearance of boundary layers. We show in Figure 3 the steady-state solution of the hyperbolic model by using the proposed DG method and the solution of the standard

DOI: 10.1002/nme

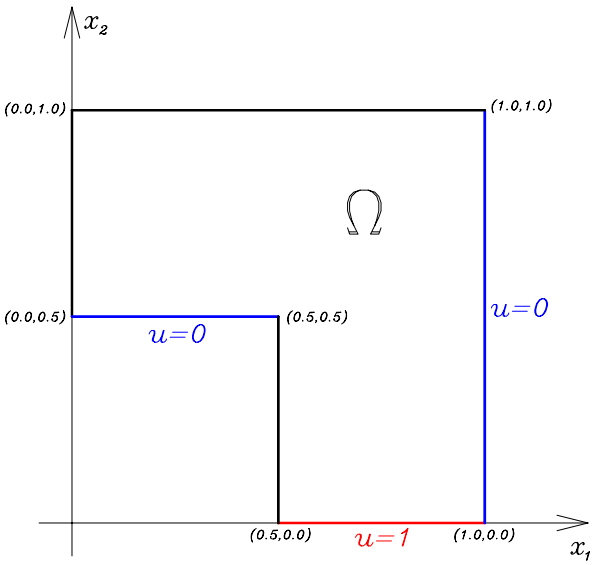

Figure 2. Pure rotation in an irregular domain. Statement of the problem. $k = 10^{-6}$, $\mathbf{a} = (-x_2, x_1)$. For the hyperbolic model $\tau = 1$.

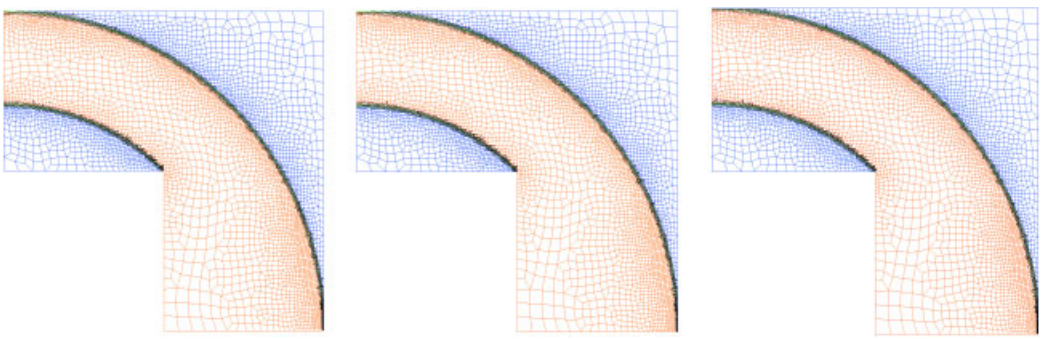

Figure 3. Pure rotation in an irregular domain. Steady-state solution. Bassi–Rebay (left), LDG (centre) and hyperbolic model (right). $k = 10^{-6}$, $\mathbf{a} = (-x_2, x_1)$. For the hyperbolic model $\tau = 1$.

parabolic model by using the LDG method and the Bassi–Rebay scheme. The computational mesh has been adapted to the steady-state solution. It has been generated by using the code GEN4U by Sarrate and Huerta [26] and it is composed of 4601 biquadratic elements. In Figure 4 we show a detail of the inflow boundary. In Figure 5 we show a detail of the discontinuity that comes up around the corner. As it can be seen in Figures 4 and 5, the discontinuities are very well resolved (one interior cell). From these examples we conclude that the numerical solution of the hyperbolic model is almost equal to the numerical solution of the parabolic model. This fact happens because we impose the condition $\mathbf{q} \cdot \mathbf{n} = 0$ on the outflow boundary for the parabolic model. If a

DOI: 10.1002/nme

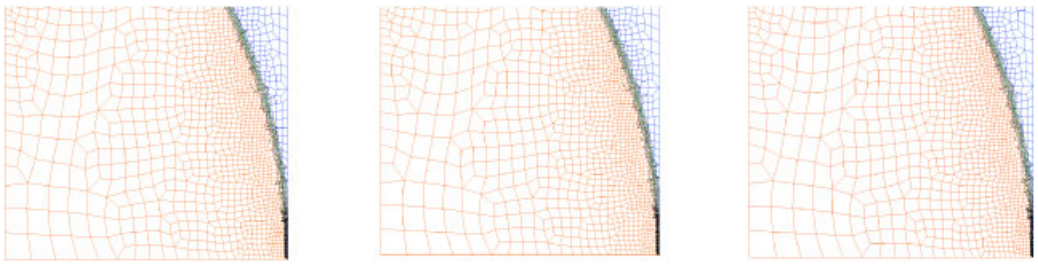

Figure 4. Pure rotation in an irregular domain. Steady-state solution. Detail of the inflow boundary. Bassi–Rebay (left), LDG (centre) and hyperbolic model (right). $k = 10^{-6}$, $\mathbf{a} = (-x_2, x_1)$. For the hyperbolic model $\tau = 1$.

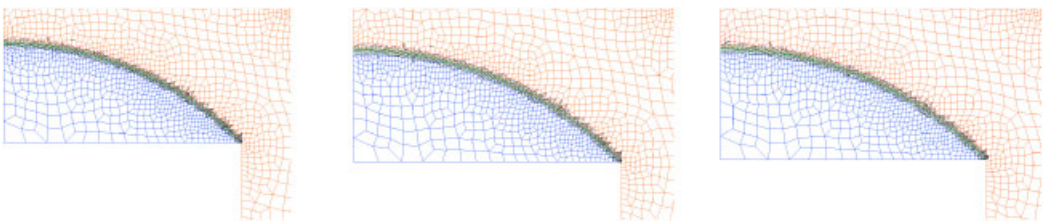

Figure 5. Pure rotation in an irregular domain. Steady-state solution. Detail of the corner. Bassi–Rebay (left), LDG (centre) and hyperbolic model (right). $k = 10^{-6}$, $\mathbf{a} = (-x_2, x_1)$. For the hyperbolic model $\tau = 1$.

Dirichlet-type condition were enforced on the outflow boundary for the parabolic model, the error of the numerical solution would be much greater and the hyperbolic model would be clearly superior. One may also argue that this is revealing the need for the appropriate boundary conditions for the parabolic problem.

5.2.2. Advection skew to the mesh. The problem setup is described in Figure 6. The computational domain is the square $[0, 1] \times [0, 1]$. Within this domain we define a computational mesh of 20×20 square biquadratic elements. So, the side length of the elements is $h = 0.02$. Taking into account all of this, we can compute the element Peclet number $Pe = \|\mathbf{a}\| h/(2k) = 25\,000$. For the hyperbolic model we must prescribe all the unknowns on the inflow boundary while no boundary conditions must be imposed on the outflow border. On the inflow boundary we enforce $\mathbf{q} = 0$ and the discontinuous boundary condition depicted in Figure 6. For the parabolic model it is necessary to impose one boundary condition everywhere on the boundary of the domain. On the outflow boundary we impose $\mathbf{q} \cdot \mathbf{n} = 0$ while the discontinuous concentration boundary condition depicted in Figure 6 has been imposed on the inflow border. The steady-state solutions for $\alpha = \arctan(1) = 45°$ and $\alpha = \arctan(2) \approx 63.43°$ are plotted in Figures 7 and 8.

As it happened in the previous example, the numerical solutions are almost equal. The reason is, again, the same.

DOI: 10.1002/nme

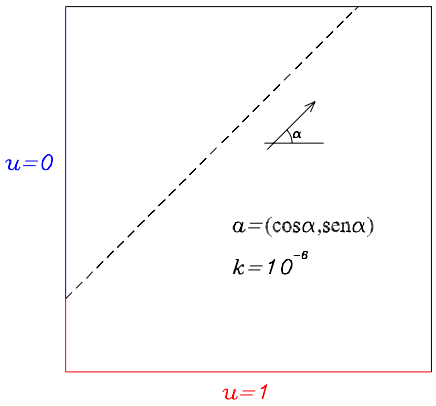

Figure 6. Advection skew to the mesh. Problem setup. $k = 10^{-6}$, $\mathbf{a} = (\cos\alpha, \sin\alpha)$. For the hyperbolic model we take $\tau = 1$.

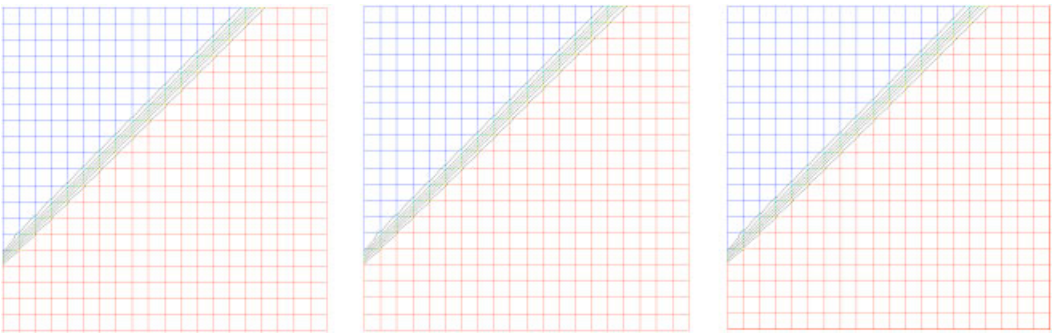

Figure 7. Advection skew to the mesh. Steady-state solution. Bassi–Rebay (left), LDG (centre) and hyperbolic model (right). $k = 10^{-6}$, $\mathbf{a} = (\cos\alpha, \sin\alpha)$, $\alpha = \arctan(1) = 45°$. For the hyperbolic model we take $\tau = 1$.

We also solved this example taking $\tau = 10^{-3}$ for the hyperbolic model. With this value of the relaxation time the flow is still supercritical, so we imposed the same boundary conditions. The steady-state solution was almost equal to those plotted in Figures 7 and 8.

5.2.3. Rotating flow. This is an accuracy test. Classical upwind procedures exhibit excessive crosswind diffusion on this problem (see for instance [27]). The problem setup is described in Figure 9. The flow is circular about the centre of the square domain $[-1, 1] \times [-1, 1]$ with a velocity field $\mathbf{a} = (-x_2, x_1)$. Diffusivity is taken to be $k = 10^{-6}$. For the hyperbolic model we set $\tau = 1$ which makes the flow supercritical except in a small circle centred in the origin of co-ordinates. For the hyperbolic model we impose homogeneous boundary conditions (concentration and pollutant flux) on the inflow boundary whereas no boundary conditions are imposed on the outflow border. In addition, we enforce the condition $u(x_1, 0) = \sin(\pi x_1)$ on the slit $x_2 = 0$, $x_1 \in [0, 1]$. On the other hand, for the parabolic model we impose $u = 0$ everywhere on the boundary

DOI: 10.1002/nme

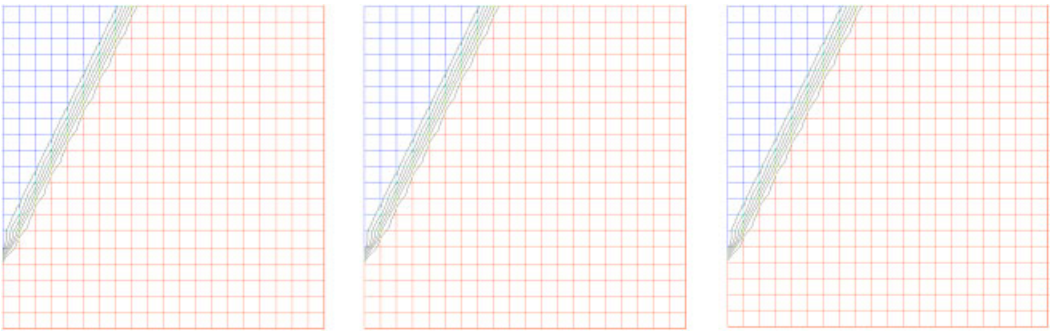

Figure 8. Advection skew to the mesh. Steady-state solution. Bassi–Rebay (left), LDG (centre) and hyperbolic model (right). $k = 10^{-6}$, $\mathbf{a} = (\cos\alpha, \sin\alpha)$, $\alpha = \arctan(2) \approx 63.43°$. For the hyperbolic model we take $\tau = 1$.

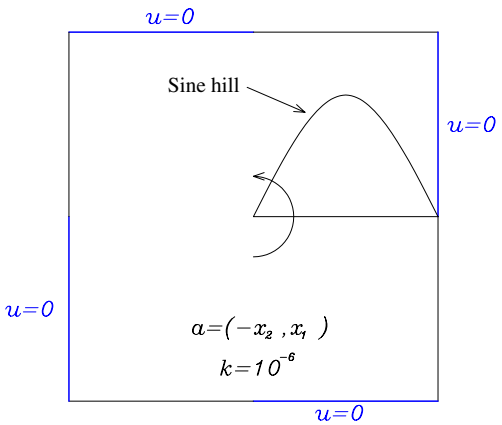

Figure 9. Rotating flow. Problem setup. $k = 10^{-6}$, $\mathbf{a} = (-x_2, x_1)$. For the hyperbolic model we take $\tau = 1$.

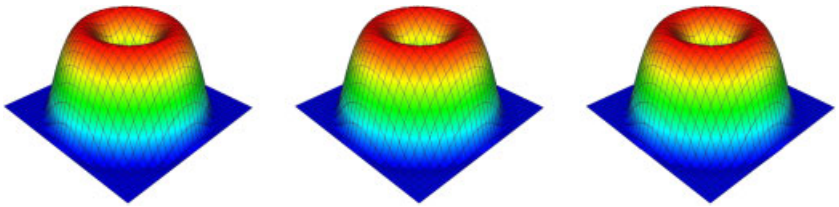

Figure 10. Rotating flow. Steady-state solution. Bassi–Rebay (left), LDG (centre) and hyperbolic model (right). $k = 10^{-6}$, $\mathbf{a} = (-x_2, x_1)$. For the hyperbolic model we take $\tau = 1$.

and the condition $u(x_1, 0) = \sin(\pi x_1)$ on the slit. Computations were done on a 30×30 uniform mesh of biquadratic square elements. The steady-state solutions are plotted in Figure 10. In Figure 11 we plot the solutions at $x_2 = 0$. All the solutions are very accurate and there is no appearance of crosswind diffusion.

DOI: 10.1002/nme

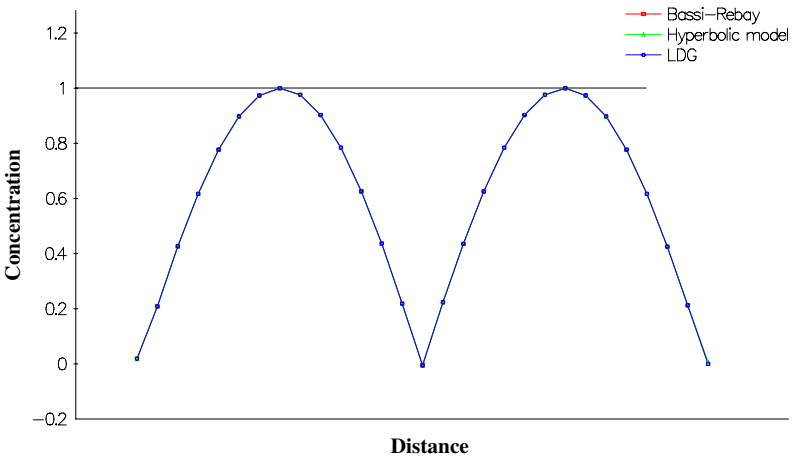

Figure 11. Rotating flow. Steady-state solutions at $x_2 = 0$. Bassi–Rebay (squares), LDG (circles) and hyperbolic model (triangles). $k = 10^{-6}$, $\mathbf{a} = (-x_2, x_1)$. For the hyperbolic model we take $\tau = 1$.

Figure 12. Simulation of an accidental spillage in the port of A Coruña, digital photograph showing the port.

6. AN APPLICATION EXAMPLE: SIMULATION OF AN ACCIDENTAL SPILLAGE IN THE PORT OF A CORUÑA

In this section we analyse the evolution of an accidental spillage in the port of A Coruña (northwest of Spain, EU) [28]. The domain comprises the whole area of the port. In Figure 12 we show a digital photograph of the port. We represent the layout of the port in Figure 13. To bound the

DOI: 10.1002/nme

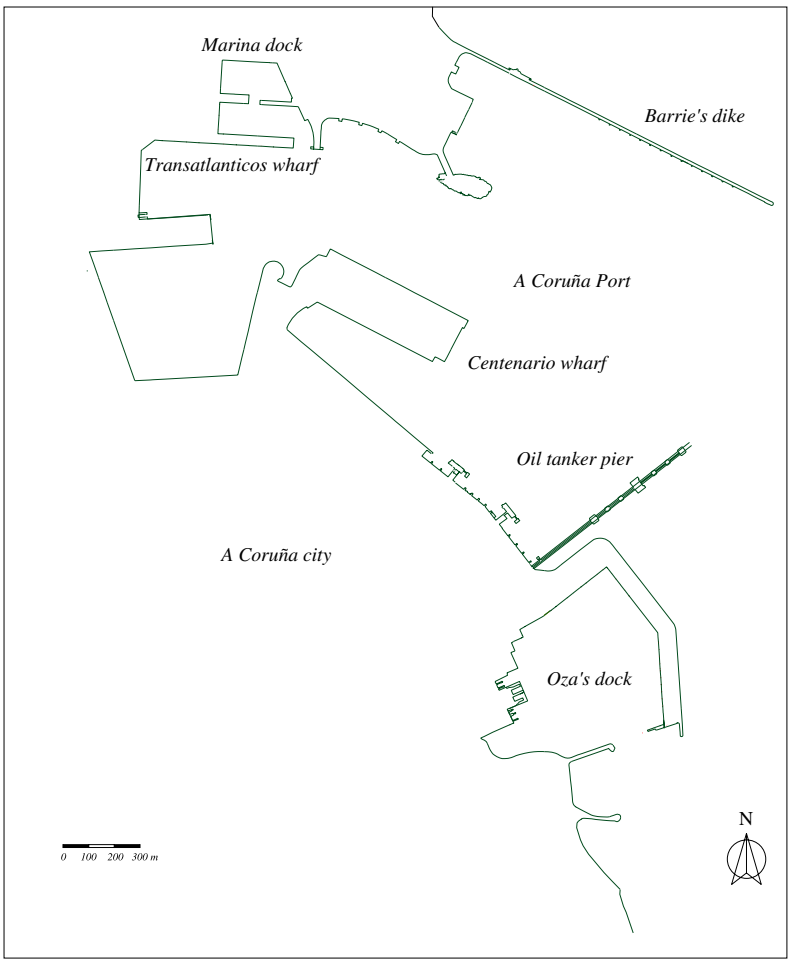

Figure 13. Simulation of an accidental spillage in the port of A Coruña. Layout of the port.

domain of the problem we define an open sea boundary from the end of Barrie's dike to the extreme of Oza's dock (see Figure 13). The resulting computational domain has been depicted in Figure 14 (left). As it can be seen in this figure, some elements of the real domain have been removed in order to simplify the generation of the mesh. Obviously, the omission of these elements is not important for the solution of the problem. For instance, the oil tanker pier allows both water and pollutant flowing through it. Therefore, it does not modify the solution.

Three kinds of boundaries are shown in Figure 14 (left): the solid wall boundary has been plotted in green; the boundary where the spillage happens has been plotted in red; the open sea boundary has been plotted in blue.

The objective of this example is to show that the proposed methodology can be used to simulate real engineering problems. For this reason we have not considered necessary to perform an accurate

DOI: 10.1002/nme

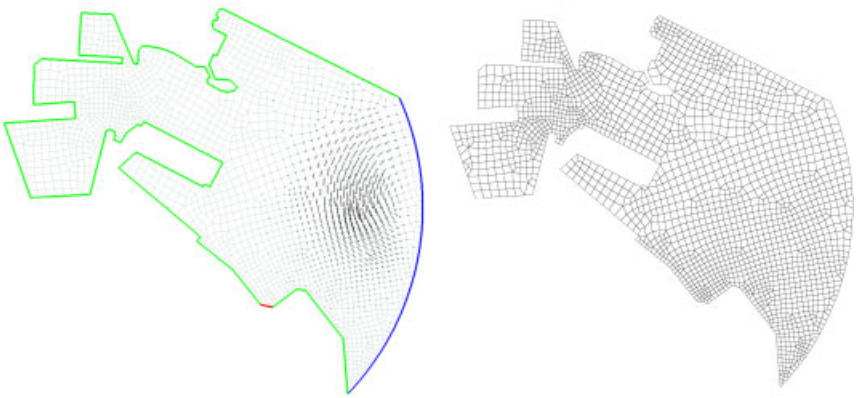

Figure 14. Simulation of an accidental spillage in the port of A Coruña. Velocity field and kinds of boundaries (left) and computational mesh of the problem (right). On the left-hand side the solid wall boundary has been plotted in green; the boundary where the spillage happens has been plotted in red; the open sea boundary has been plotted in blue. The finite element mesh consists of 2023 biquadratic elements and it was generated by using the code GEN4U [26].

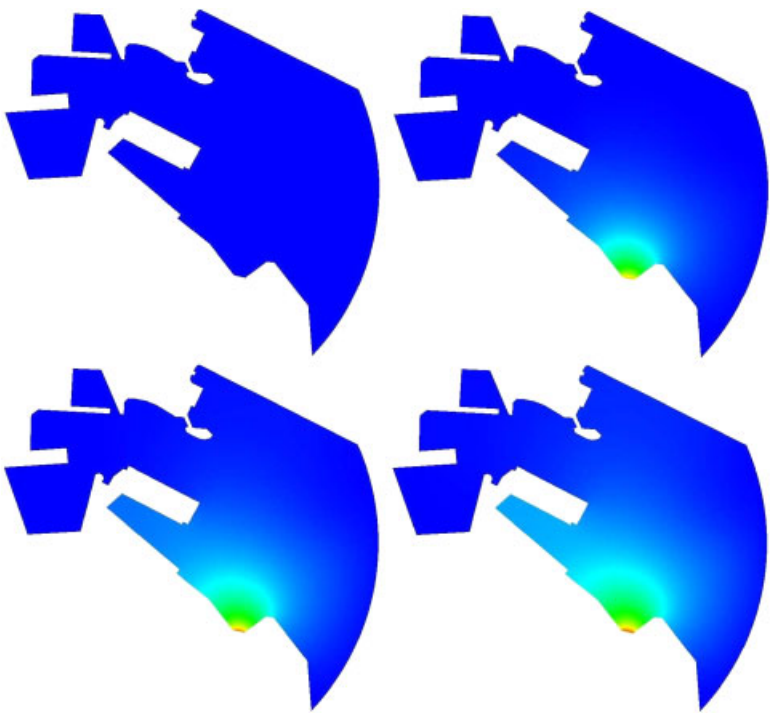

Figure 15. Simulation of an accidental spillage in the port of A Coruña. We show (left to right and top to bottom) the concentration initial condition and concentration solutions at non-dimensional times $t^* = 25$, 50 and 75.

DOI: 10.1002/nme

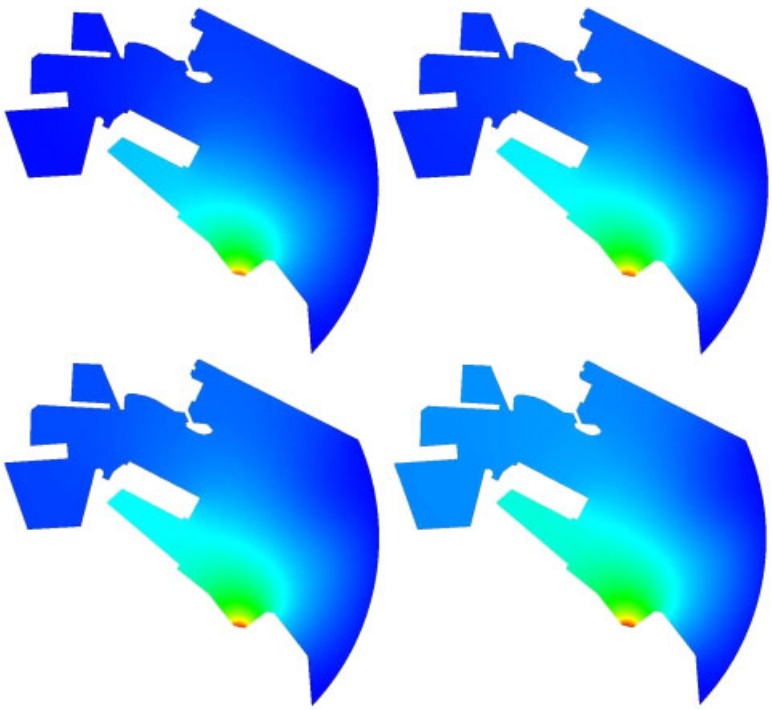

Figure 16. Simulation of an accidental spillage in the port of A Coruña. We show (left to right and top to bottom) concentration solutions at non-dimensional times $t^* = 100$, 150, 200 and 400.

estimation of the parameters which would entail a lot of experimental work. A typical value for engineering calculations has been selected for the diffusivity k [29]. The estimation of the relaxation time τ is not so trivial since only the order of magnitude of the parameter can be estimated without making experiments. However, what really determines the solution is the velocity of the fluid $\mathbf{a}$ with respect to the velocity of the pollutant $c = \sqrt{k/\tau}$. This quotient defines a Mach-type number as it can be seen in Equation (21).

In order to reduce the computations, the velocity field has not been calculated, but it was generated with two constraints: (a) it verifies pointwise the continuity equation for incompressible flow and (b) it satisfies standard boundary conditions for a viscous flow. The velocity field has been plotted in Figure 14 (left). On the right-hand side of Figure 14 we have depicted the computational mesh which is composed of 2023 biquadratic elements.

On the solid wall boundary we impose $\mathbf{q} \cdot \mathbf{n} = 0$. On the boundary where the spillage takes place the condition $\mathbf{q} \cdot \mathbf{n} = -10^{-2}$ is imposed. On the open sea boundary we impose $\mathbf{q} \cdot \mathbf{n} = cu$ where $c = \sqrt{k/\tau}$ is the pollutant wave velocity. The flow is given by H numbers (see definition in Equation (21)) verifying $H \leqslant H_{\max} \approx 0.3237$ what makes the problem to be subcritical at each point of the domain.

At this point we define the non-dimensional time $t^* = t/\tau$. In Figure 15 we show the initial concentration and concentration solutions at non-dimensional times $t^* = 25$, 50 and 75. In Figure 16 concentration solutions at non-dimensional times $t^* = 100$, $t^* = 150$, 200 and 400 are plotted.

DOI: 10.1002/nme

7. CONCLUSIONS

In this paper we present a hyperbolic model for convection–diffusion problems in CFD based on Cattaneo's law. The Cattaneo-type formulation avoids the infinite speed paradox that is inherent in the standard parabolic formulation. The proposed formulation constitutes a generalized approach for convective–diffusive phenomena since the standard formulation can be considered as a subcase of the proposed one.

A high-order upwind DG method has been developed and applied to the resolution of classic convection-dominated test problems. The results have been compared with those obtained by using the parabolic model and the Bassi–Rebay scheme or the LDG method. We conclude that the results are very similar when the normal pollutant flux is enforced to vanish on the outflow boundary for the parabolic model. If a Dirichlet-type condition were imposed on the outflow boundary for the parabolic model, the proposed model would be superior.

The proposed DG method for the hyperbolic model presents other convenient properties: the domain of dependence of the method is minimal (this is not the case for the parabolic model; however, in parabolic equations solved with explicit methods fluxes can be eliminated at the element level) and the optimal orders of accuracy are achieved in both, concentration and pollutant flux (it is known that the DG method converges at optimal rate for hyperbolic equations).

Finally, we solve an application example to show the performance of the mathematical model and of the numerical model. This example concerns the evolution of a pollutant being spilled in the port of A Coruña (northwest of Spain, EU).

ACKNOWLEDGEMENTS

This work has been partially supported by Grant Numbers PGIDT03PXIC18001PN and PGIDT05PXIC-18002PN of the "Subdirección Xeral de I+D de la Xunta de Galicia", by Grant Numbers DPI2002-00297 and DPI2004-05156 of the "Ministerio de Educación y Ciencia", and by research fellowships of the "Universidade da Coruña" and the "Fundación de la Ingeniería Civil de Galicia".

REFERENCES

1. Reed WH, Hill TR. Triangular mesh methods for the neutron transport equation. *Technical Report LA-UR-73-479*, Los Alamos Scientific Laboratory, 1973.
2. Cockburn B, Karniadakis GE, Shu C-W (eds). *Discontinuous Galerkin methods. Theory*, *Computation and Applications*. Springer: Berlin, 1999.
3. Cockburn B, Shu C-W. TVB Runge–Kutta local projection discontinuous Galerkin finite element method for scalar conservation laws II: general framework. *Mathematics of Computation* 1989; **52**:411–435.
4. Cockburn B, Lin S-Y, Shu C-W. TVB Runge–Kutta local projection discontinuous Galerkin finite element method for conservation laws III: one-dimensional systems. *Journal of Computational Physics* 1989; **84**:90–113.
5. Cockburn B, Shu C-W. The Runge–Kutta discontinuous Galerkin finite element method for conservation laws V: multidimensional systems. *Journal of Computational Physics* 1998; **141**:199–224.
6. Cockburn B, Shu C-W. Runge–Kutta discontinuous Galerkin methods for convection dominated flows. *Journal of Scientific Computing* 2001; **16**(3):173–261.
7. Bassi F, Rebay S. A high-order accurate discontinuous finite element method for the numerical solution of the compressible Navier–Stokes equations. *Journal of Computational Physics* 1997; **131**:267–279.
8. Cockburn B, Shu C-W. The local discontinuous Galerkin method for time-dependent convection–diffusion systems. *SIAM Journal on Numerical Analysis* 1998; **35**(6):2440–2463.
9. Baumann CE, Oden JT. A discontinuous *hp* finite element method for convection–diffusion problems. *Computer Methods in Applied Mechanics and Engineering* 1999; **175**:311–341.

DOI: 10.1002/nme

10. Baumann CE, Oden JT. A discontinuous *hp* finite element method for the Euler and the Navier–Stokes equations. *International Journal for Numerical Methods in Engineering* 1999; **31**:79–95.
11. Castillo P. Performance of discontinuous Galerkin methods for elliptic PDEs. *SIAM Journal on Scientific Computing* 2002; **24**(2):524–547.
12. Castillo P, Cockburn B, Perugia I, Schötzau D. An a priori error analysis of the local discontinuous Galerkin method for elliptic problems. *SIAM Journal on Numerical Analysis* 2000; **38**(5):1676–1706.
13. Cattaneo MC. Sulla conduzione de calore. *Atti del Seminario Matematico e Fisico dell Univ di Modena* 1948; **3**:83–101.
14. Cattaneo MC. Sur une forme de l'equation de la chaleur éliminant le paradoxe d'une propagation instantaneé. *Comptes Rendus de L'Academie des Sciences*: *Series I-Mathematics* 1958; **247**:431–433.
15. Courant R, Hilbert D. *Methods of Mathematical Physics*, vol. II. Wiley: New York, 1989.
16. Gómez H. A new formulation for the advective–diffusive transport problem. *Technical Report* (in Spanish), University of A Coruña, 2003. http://caminos.udc.es/gmni/index.html
17. Christov CI, Jordan PM. Heat conduction paradox involving second-sound propagation in moving media. *Physical Review Letters* 2005; **94**(15):4301–4304.
18. Gómez H. A hyperbolic formulation for convective–diffusive problems in CFD. *Ph.D. Dissertation* (in Spanish), University of A Coruña, 2006.
19. Gómez H, Colominas I, Navarrina F, Casteleiro M. A generalized method for advective–diffusive computations in engineering. In *Fluid Structure Interaction and Moving Boundary Problems*, Chakrabarti SK, Hernández S, Brebbia CA (eds), 2005; 563–573.
20. Gómez H, Colominas I, Navarrina F, Casteleiro M. A finite element formulation for a convection–diffusion equation based on Cattaneo's law. *Computer Methods in Applied Mechanics and Engineering* 2007; **196**(9–12): 1757–1766.
21. Courant R, Friedrichs KO. *Supersonic Flow and Shock Waves*. Springer: Berlin, 1999.
22. Whitham GB. *Linear and Nonlinear Waves*. Wiley: New York, 1999.
23. Shu C-W, Osher S. Efficient implementation of essentially non-oscillatory shock-capturing schemes. *Journal of Computational Physics* 1988; **77**:439–471.
24. Bazilevs Y, Hughes TJR. Weak imposition of Dirichlet boundary conditions in fluid mechanics. *Computers and Fluids* 2007; **36**(1):12–26.
25. Hughes TJR, Scovazzi G, Bochev PB, Buffa A. A multiscale discontinuous Galerkin method with the computational structure of a continuous Galerkin method. *Computer Methods in Applied Mechanics and Engineering* 2006; **195**:2761–2787.
26. Sarrate J, Huerta A. Efficient unstructured quadrilateral mesh generation. *International Journal for Numerical Methods in Engineering* 2000; **49**:1327–1350.
27. Brooks A, Hughes TJR. Streamline upwind/Petrov–Galerkin formulations for convection dominated flows with particular emphasis on the incompressible Navier–Stokes equations. *Computer Methods in Applied Mechanics and Engineering* 1982; **32**(1–3):199–259.
28. Figueroa CA, Colominas I, Mosqueira G, Navarrina F, Casteleiro M. A stabilized finite element approach for advective–diffusive transport problems. In *Proceedings of the XX Iberian Latin-American Congress on Computational Methods in Engineering* (CDROM), Pimenta PM, Brasil R, Almeida E (eds), São Paulo, Brasil, 1999.
29. Holley ER. Diffusion and dispersion. In *Environmental Hydraulics*, Singh VP, Hager WH (eds). Kluwer Academic Publishers: Dordrecht, 1996; 111–151.

DOI: 10.1002/nme